frontiers | Frontiers in Materials

TYPE Original Research
PUBLISHED 14 March 2023
DOI 10.3389/fmats.2023.1129886

OPEN ACCESS

EDITED BY
Zhiming Zhang,
Institute of Corrosion Science and Technology, China

REVIEWED BY
Jihui Wang,
Tianjin University, China
Long HAO,
Corrosion and Protection Center of Materials, Institute of Metal Research (CAS), China

*CORRESPONDENCE
Tsung-Kuang Yeh,
tkyeh@mx.nthu.edu.tw

SPECIALTY SECTION
This article was submitted to Environmental Degradation of Materials, a section of the journal Frontiers in Materials

RECEIVED 22 December 2022
ACCEPTED 27 February 2023
PUBLISHED 14 March 2023

CITATION
Sathasivam K, Wang M-Y, Anbalagan Ak, Lee C-H and Yeh T-K (2023), Novel photocatalytic coating for corrosion mitigation in 304LSS of dry storage canisters.
Front. Mater. 10:1129886.
doi: 10.3389/fmats.2023.1129886

Novel photocatalytic coating for corrosion mitigation in 304LSS of dry storage canisters

Kamalasekaran Sathasivam[1,2], Mei-Ya Wang[3], Aswin kumar Anbalagan[2], Chih-Hao Lee[2,4] and Tsung-Kuang Yeh[2,4]*

[1]Nanoscience and Technology Program, Taiwan International Graduate Program, Academia Sinica, Taipei, Taiwan, [2]Department of Engineering and System Science, National Tsing Hua University, Hsinchu, Taiwan, [3]Nuclear Science and Technology Development Center, National Tsing Hua University, Hsinchu, Taiwan, [4]Institute of Nuclear Engineering and Science, National Tsing Hua University, Hsinchu, Taiwan

Type 304L stainless steel (304LSS) is one of the candidate canister materials for storing radioactive spent fuels, usually near seashore environments along with nuclear power plants. During the prolonged exposure of dry storage canisters to saline environments, they are highly susceptible to chloride induced stress corrosion cracking. Failure of a dry storage canister not only would release radioactive isotopes into the environment, but would also lead to a costly replacement of the cracked canister. The objective of this study is to develop a multilayered titanium dioxide (TiO_2) composite coating on a 304LSS substrate. With ultraviolet (UV) illumination, this coating would act as a barrier and simultaneously offer cathodic protection against corrosion in the substrate alloy. The composite coating consists of a plain amorphous TiO_2 coating over another cerium-doped (Ce-doped) TiO_2 coating. Electronic currents generated by photo-catalytic reaction of the amorphous TiO_2 coating under UV illumination were measured. Photo-electrochemical analyses and surface morphology observations were conducted to evaluate the performance of the Ce-doped coatings on corrosion mitigation. Optimal amounts of cerium doping that offered better photo-cathodic protection were also explored. Results indicated that the Ce-doped TiO_2 coating exhibited a better performance on photo-cathodic protection for 304L stainless steel in aerated 3.5% NaCl solutions than the one without cerium doping. The underlying Ce-doped TiO_2 coating was effectively charged during UV illumination, and it was able to continuously release electrons even after the UV was switched off, thus providing uninterrupted photo-cathodic protection for the coated 304L stainless steel substrate.

KEYWORDS

dry storage canister, 304L stainless steel (304LSS), titanium dioxide (TiO_2), cerium doping, photo-cathodic protection

1 Introduction

Although nuclear power is a sustainable source of energy with low carbon emissions (Saito, 2010), it generates long half-life radioactive spent fuels that require careful monitoring and safe storage (Zhang et al., 2020). Dry storage canisters are used to temporarily store the spent fuels prior to their final disposal or reprocessing (Wang et al., 2020). For the manufacturing of canisters, austenitic stainless steel grades such as 304 and 316 are generally used as the base materials (Wang et al., 2022). While the anticipated storage

time of the canisters is around 40 years, they require periodic inspection and careful maintenance to prevent radioactive substances from leaching into the environment. The long-term integrity and corrosion resistance of the canisters depends on several factors such as temperature, humidity, brine concentration in the marine environment, and residual stresses in the canisters induced by welding (Yeom and Sridharan, 2021). In general, during long-term exposures to a marine environment, the steel canisters are likely to suffer from chloride-induced stress corrosion cracking (CISCC). Deteriorations in the canisters may lead to a safety issue if radionuclides escape to the environment of the dry storage site (Yeom et al., 2020). Mitigating CISCC is, therefore, necessary to ensure safety and extend the canisters' service lives.

To enhance the corrosion resistance of 304LSS, one proven technique is to apply ceramic coatings such as titanium dioxide (TiO_2) together with ultraviolet (UV) illumination (Sathasivam et al., 2022). Although the coating acts as an effective barrier by reducing contact between the metal and the corrosive marine environment, it requires high processing temperatures for enhanced photocatalytic activity and surface adherence. However, post-thermal treatment processes increase production costs and are often incompatible with the structural alloys (Subasri and Shinohara, 2004). To overcome these shortcomings, researchers have explored low-temperature amorphous TiO_2 coatings with enhanced photocatalytic activity (Shinohara, 2001). An amorphous TiO_2 coating may offer photo-cathodic protection on the coated metal only during UV illumination by generating excess free electrons. Upon the switch off of UV illumination, the coating would fail to protect the substrate metal due to the recombination of the photogenerated electrons and the existing holes, which eventually limits their industrial applications (Li et al., 2005). Researchers have tried to overcome these problems, using semiconductor coupling (Liu et al., 2014), metal doping (Momeni and Motalebian, 2021), and non-metal doping (Li et al., 2010), but most focused on improving photoelectric efficiency rather than on charge storage and discharge capabilities of TiO_2. In addition, these technologies require complex experimental setups, rendering them impractical for onsite industrial applications. For practical applications, it is therefore necessary to develop an appropriate TiO_2 nanocomposite system with charge storage capability at low processing temperatures.

Rare Earth elements such as cerium and lanthanum are widely used to improve the long-term corrosion resistance of the canisters' structural material (Peng et al., 2018). Among the additives, cerium nitrate salts are considered effective inhibitors due to their desired properties, low cost, low toxicity, eco-friendliness, and availability (Li et al., 2012). Also, cerium ions precipitate to form cerium oxides or hydroxides that prohibit cathodic and anodic reactions in the canisters' defects (Yang and Cheng, 2017). Furthermore, cerium oxides are chiefly used as alternative electrode material in supercapacitors (Padmanathan and Selladurai, 2014). The redox couple of the cerium oxide Ce^{3+}/Ce^{4+} improves the charge separation of electrons and holes and suppresses their recombining with electron trapping at Ce^{4+} ions. Thus, the redox couple acts as an electron storage pool, which indicates that cerium oxide is an effective material for electron storage during the photo-cathodic protection process. Even so, using cerium oxide as an energy storage material for photo-cathodic protection has thus far proved unsuccessful. While researchers have investigated the use of CeO_2 on the TiO_2 outer layer for the photo-cathodic protection of copper, they have found that the prepared coating cannot trap and store the photogenerated electrons in an aerated 0.3% NaCl solution (Subasri and Shinohara, 2003).

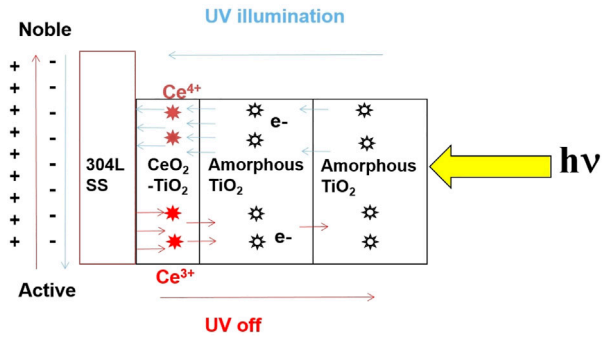

FIGURE 1
Schematic representation of 2 layers of amorphous TiO_2/Ce doped TiO_2 coatings on a 304LSS substrate and the working principle of photocathodic protection on the substrate under UV illumination.

The present study is the first to investigate the multilayered CeO_2 doped TiO_2 coating with various concentrations of cerium ions to provide sufficient photo-cathodic protection and electron storage capacity in a 3.5% NaCl solution.

Open circuit potential and electrochemical polarization were performed to evaluate the electrochemical properties of the coated 304LSS. The photo-cathodic protection performance for coated 304LSS in a NaCl solution was demonstrated in the presence and absence of stimulated UV illumination. The present investigation develops not only a novel photocatalytic coating but also lays the foundation for a promising new field—long-term photo-cathodic metal protection.

Figure 1 shows the working principle of the multilayered Ce-doped TiO_2 coatings. The strategy behind applying a TiO_2 coating over the photo cathodic protection of 304LSS is to supply excess electrons under stimulated UV illumination, which results in a higher negative electrode potential than the stainless steel's corrosion potential. However, due to the high recombination kinetics of the charge carriers, this type of photocatalytic coating retains its function only in the presence of UV illumination. By developing a novel composite coating and incorporating another semiconductor material to store the ample electrons generated by the TiO_2 coating during UV illumination (which retains the cathodic protection of the metal in dark conditions), we circumvented the shortcomings of the plain TiO_2 coatings.

The proposed design of the multilayer TiO_2 coating consists of an inner layer of cerium-doped TiO_2, followed by two outer layers of amorphous plain TiO_2 coatings. Cerium oxide is a well-known n-type semiconductor candidate material with a band gap of 2.9 eV and an appreciable reductive energy storage property (Zhang et al., 2012). Although the cerium-doped TiO_2 was fabricated as an inner layer that acts as an electron scavenger to preserve the surplus electrons generated under simulated UV illumination, the photocatalytic effect from this layer is

TABLE 1 Annealing treatment conditions for Ce doped TiO_2 and plain TiO_2 coatings over 304LSS.

Designated name	Coating layers	Temperature (°C)	Annealing environment	Flow rate (SCCM)
304LSS/1TO	304LSS/amorphous TiO_2	200	Argon	176
304LSS/2TO-10-Ce	304LSS/amorphous TiO_2/10% Ce-TiO_2	200/200	Argon	176
304LSS/2TO-20-Ce	304LSS/amorphous TiO_2/20% Ce-TiO_2	200/200	Argon	176
304LSS/2TO-30-Ce	304LSS/amorphous TiO_2/30% Ce-TiO_2	200/200	Argon	176
304LSS/3TO-30-Ce	304LSS/amorphous TiO_2/amorphous TiO_2/30% Ce-TiO_2	200/200/200	Argon	176

TABLE 2 Annealing treatment conditions for Ce doped TiO_2 and plain TiO_2 coatings over ITO.

Designated name	Coating layers	Temperature (°C)	Annealing environment	Flow rate (SCCM)
ITO (AM)/1TO	ITO/amorphous TiO_2	200	Argon	176
ITO/2TO-10-Ce	ITO/amorphous TiO_2/10% Ce-TiO_2	200/200	Argon	176

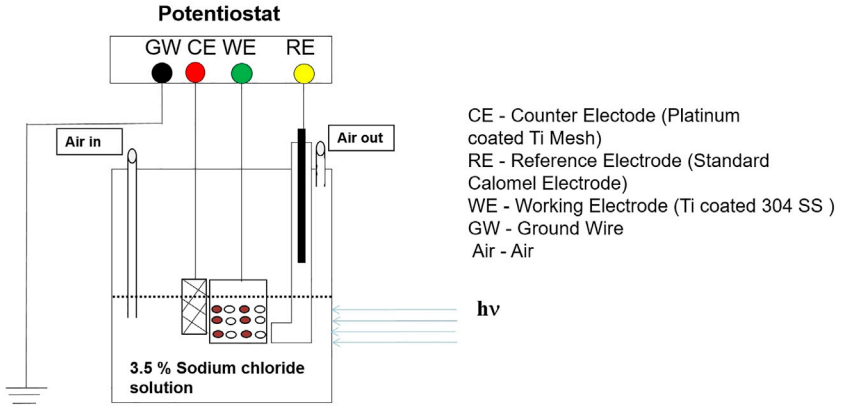

FIGURE 2
Schematic of a three electrode photoelectrochemical system with a potentiostat for polarization analyses.

insufficient to make the open circuit potential of 304LSS the more active value for the metal's effective protection. Hence it is necessary to overlay this charge storage layer with several layers of the amorphous TiO_2 coating. During UV illumination, these layers act as free electron donors and serve as a barrier that inhibits the stored electrons from escaping from the inner Ce-doped TiO_2 layers once the UV illumination is turned off.

Cerium oxide has a multivalence state of +3 and +4 in which the Ce^{4+} ions undergo a partial reduction reaction and transit to Ce^{3+} *via* the faradaic intercalation of cations that trap a portion of the photogenerated electrons from the outer amorphous TiO_2 coating under UV illumination. Moreover, compared to TiO_2, CeO_2 has superior electrical conductivity, which facilitates the smooth charge transfer of the remaining photoelectrons from the outer amorphous TiO_2 coating to reach the 304LSS substrate. This results in a significant effective photo-cathodic protection of the metal alloys. When the UV illumination is turned off, the reduced Ce^{3+} ions tend to re-oxidize into Ce^{4+} by releasing stored electrons through oxygen reduction reactions. The released electrons from the metastable low-valence Ce^{3+} ions retain the photo-cathodic protection of the metal alloys even in the absence of UV illumination. Furthermore, the overlaid two layers of amorphous TiO_2 coating act as an effective barrier to prevent the transport of stored electrons from the coatings and interacting directly with the oxidizing species in the electrolyte medium. Eventually, the electrochemical corrosion potential of the coated substrate displayed a linear anodic shift rather than a fast recovery to the aboriginal electrode potential once the UV illumination is turned off. This modified Ce-doped multilayered TiO_2 coating exhibits unique characteristics of electron storage and release (see Figure 1), which may help to deliver effective photo-cathodic protection for an extended period even in the absence of UV illumination. The principal mechanism of electron trapping and releasing is as follows (Tong et al., 2007):

Trapping: $Ce^{4+}e^- \longrightarrow Ce^{3+}$

Releasing: $Ce^{3+} \longrightarrow Ce^{4+}e^-$

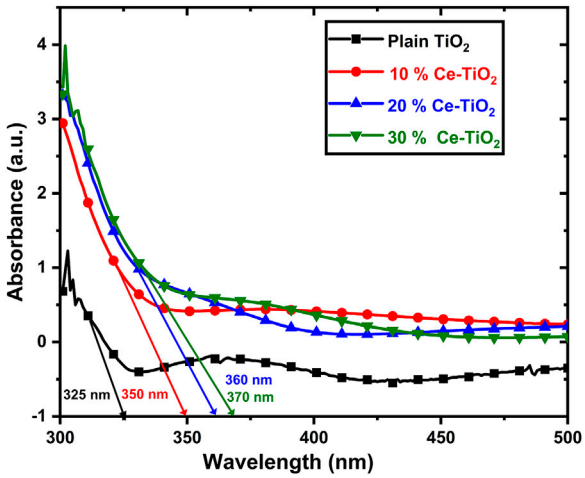

FIGURE 3
UV-visible absorption spectra for plain TiO_2 and various concentrations of Ce doped TiO_2 thin films on ITO glass.

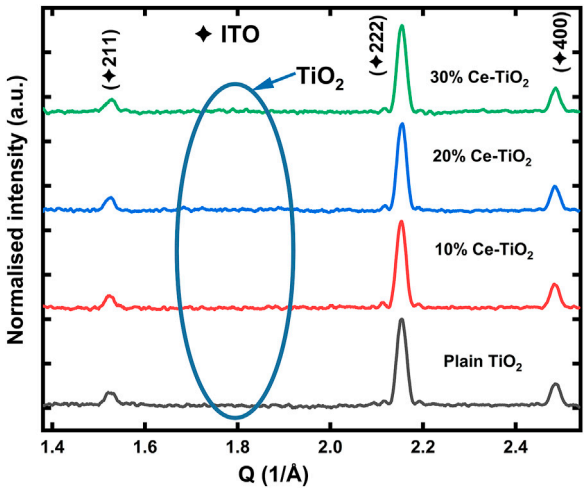

FIGURE 4
XRD analysis results of the annealed TiO_2 coating and various concentrations of Ce doped TiO_2 thin films on ITO glass.

2 Experimental

2.1 TiO_2 solgel preparation

The sol-gel synthesis process was used to prepare two types of TiO_2 coating: a cerium-doped TiO_2 sol-gel and plain amorphous TiO_2 prepared separately with different operating parameters. Sigma Aldrich supplied the necessary reagents of analytical grade, which were used without further purification.

2.1.1 Ce-doped TiO_2 sol-gel preparation

A Ce-doped TiO_2 sol-gel solution with different weight percentages of cerium (10%, 20%, and 30%) was prepared using titanium isopropoxide and cerium III) nitrate as precursors and ethanol as the solvent. An appropriate concentration of cerium nitrate was dissolved in 10 ml of ethanol to form a cerium nitrate solution. The prepared solution was later added slowly to the titanium isopropoxide solution with constant magnetic stirring at 0°C in an ice bath. The resultant yellowish-brown transparent solution was aged and used as the Ce-doped TiO_2 precursor solution.

2.1.2 Plain amorphous TiO_2 sol-gel preparation

The amorphous TiO_2 sol-gel solution for the photo cathodic protection application consisted of a mixed composition of 7.5 g of titanium tetra isopropoxide precursor (97%), 2.9 g of anhydrous ethanol, 1.8 g (65%) of nitric acid, and an additional 8 g of ethanol. The ethanol solution was cooled for 24 h before the experiment. The first two reagents were mixed at a constant stirring condition (80 rpm) in an ice bath for 10 min. The latter was then added to the premixed solution to form a homogeneous sol-gel solution. The solution temperature was maintained at 0°C *via* the sol-gel synthesis process. The resulting transparent sol-gel solution was aged and used as the amorphous TiO_2 coating for the 304LSS/ITO substrate.

2.2 Substrate sample preparation

Commercially available grades of ASTM 304LSS with a square dimension of 2 cm by 2 cm by 0.5 cm were used as a substrate material. Before the coating process, these 304LSS plates were mechanically polished with SiC emery paper (up to 600 grit) and then degreased with acetone and distilled water in an ultrasonic bath for 10 min. Subsequently, the 304LSS plates were dried and blown with argon gas after cleaning. The precleaned samples were immersed in various known concentrations of Ce-doped TiO_2 and plain TiO_2 sol-gel solution *via* a commercial dip coating machine. For each layer of coating, the samples were lowered into the sol-gel solution for 1 min and then slowly withdrawn at a regulated speed of 3 mm per min. The samples coated with different concentrations of Ce-doped TiO_2 and plain amorphous TiO_2 coatings were designated as 304LSS/1TO, 304LSS/2TO-10-Ce, 304LSS/2TO-20-Ce, 304LSS/2TO-30-Ce, 304LSS/3TO-20-Ce and subjected to a thermal annealing treatment at the relatively low temperature of 200°C for 1 h in an argon environment (see Table 1) with a heating ramp rate fixed at 5°C/min for all treatments. A layer of smooth, homogenous, high-quality adhesive coating was obtained over each 304LSS sample after the annealing treatment. To investigate the photocatalytic and charge storage properties of the Ce-doped and plain TiO_2 coatings, ITO glass with the same dimensions of 304LSS was used and coated in the same way as that of the 304LSS samples for pertinent comparative studies (see Table 2). The thermally treated specimens were staged in a desiccator and then used for the photo-electrochemical measurements.

2.3 Analytical measurements of the coating properties

The photo-absorption properties of the prepared TiO_2 and Ce-doped TiO_2 coated samples were measured using an HP8453

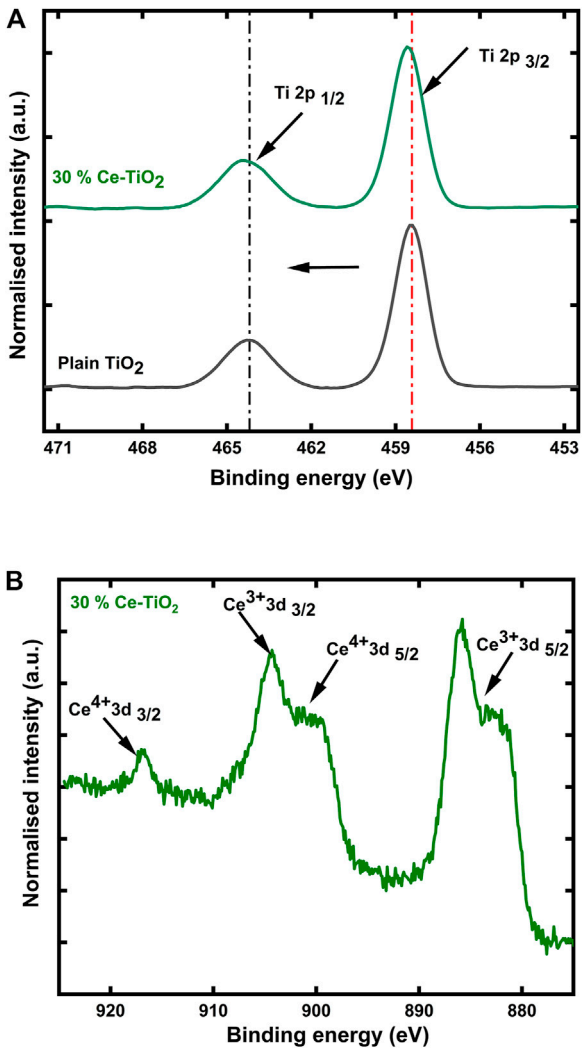

FIGURE 5
(A) Ti 2p XPS spectra of plain TiO_2 and 30% Ce doped TiO_2 samples and **(B)** Ce 3days XPS spectra of 30% Ce doped TiO_2 samples.

(HP Germany) UV-visible spectrometer at a wavelength of 300–500 nm. Glancing angle X-ray diffraction (GAXD) measurements were performed for TiO_2 and Ce-doped TiO_2 samples at the end station of the TLS - 13A beamline of the National Synchrotron Radiation Research Center Facility (NSRRC), Taiwan. The samples were measured at a glancing angle of 0.5° over a 2-theta range of 13°–24°. Furthermore, the chemical states of TiO_2 before and after Ce doping were measured using X-ray photoelectron spectroscopy (XPS, Ulvac- PHI 5000 Versa Probe II) with Al K_α excitation source. The surface morphologies of the prepared substrate samples were observed using field emission scanning electron microscopy (FE-SEM, JEOL JSM-6330F). In addition, the chemical composition of the TiO_2-coated and Ce-doped TiO_2 samples was analyzed using an energy dispersion spectroscope (EDS, Oxford INCA300, England) attached to the SEM. Both TiO_2 and Ce-doped TiO_2 coatings were prepared over the 304LSS/ITO substrates using dip-coating equipment (Sadhu design).

2.4 Electrochemical analyses

A commercial potentiostat manufactured by Corrtest Instruments was used to execute potential variation monitoring and electrochemical polarization analyses due to the impact of UV illumination on the open circuit potentials (OCPs) and corrosion current density of the multilayered Ce doped TiO_2-coated 304LSS specimen. Briefly, to simulate the ambient marine environment, electrochemical analyses were conducted at room temperature in an electrolyte solution (3.5% sodium chloride, NaCl) under aerated conditions with a pH of 7. The operating parameters for the electrochemical polarization analysis were set up in the potential window of 100mv lower and greater than the obtained equilibrium potential vs. saturated calomel electrode from the open circuit potential monitoring analysis. The potential increment or decrement was set up at 15 mv/min. Figure 2 shows the setup schematic of the custom-made three-electrode photo electrochemical system in which the TiO_2-coated 304LSS acted as a working electrode while the platinum-coated titanium mesh and saturated calomel electrode served as the counter and reference electrode, respectively. Additionally, the system was equipped with a quartz glass window to allow the UV illumination to fall on the 304LSS sample. A 500 W Hamamatsu-made (LC8) mercury-xenon lamp was used as an ideal spot UV light source to stimulate UV light with an intensity of 4,300 mW/cm^2 and a wavelength of 254 nm. Before the startup of each round of polarization analysis, all samples were immersed in the electrolyte solution for 30 min to allow the equilibrium potential to stabilize.

3 Results and discussion

3.1 Optical absorption properties of the TiO_2 coatings

The UV visible absorption spectra of the various concentrations of Ce-doped TiO_2 and plain TiO_2 coatings applied over the ITO glass substrates were measured in the wavelength range of 300–500 nm, as shown in Figure 3. Linear extrapolation was employed to determine the absorption onset wavelength of all samples. The absorption spectrum of the plain amorphous TiO_2 coatings shows strong absorption in the deep–UV region and was cut off at the absorption edge at 325 nm, while all the Ce-doped TiO_2 samples showed a progressive red shift of absorption edge with an increase in the concentration of Ce from 10% to 30%. Among the samples, the 30% Ce–doped TiO_2 exhibited the highest absorption edge at 370 nm. The most significant factor attributed to the redshift was the introduction of defect sites accompanying the Ce element in the TiO_2 matrix, which can narrow the bandgap of TiO_2(Luo et al., 2015). The results indicate that doping Ce into the TiO_2 coating significantly reduces band gap energy and effectively inhibits the recombination of the photogenerated electron holes.

3.2 XRD analysis

To characterize the crystalline nature and structure of the TiO_2 coatings under different concentrations of cerium, glancing angle X-ray diffraction (GAXD) measurements were performed. Plain and

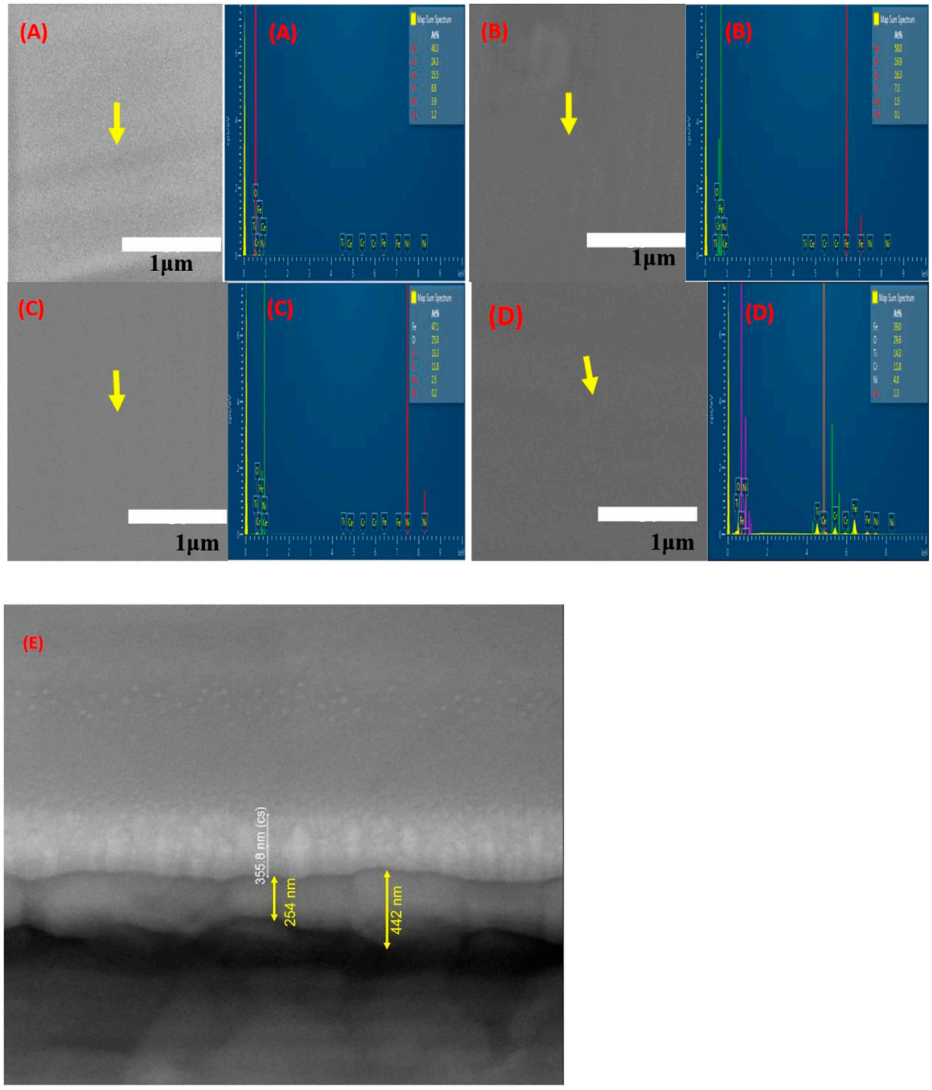

FIGURE 6
SEM images and EDX analysis results of various Ce-doped TiO_2 coatings. **(A)** 10% Ce-TiO_2 **(B)** 20% Ce-TiO_2 **(C)** 30% Ce-TiO_2 and **(D)** 304LSS/3TO-30-Ce **(E)** Cross section morphology of 304LSS/3TO-30-Ce.

Ce-doped samples coated over ITO substrates were annealed at 200°C for 1 h. Figure 4, shows the GAXD pattern of the various concentrations of the plain and Ce-doped TiO_2 samples plotted in reciprocal space q ($q = 4\pi sin\ \theta/\lambda$), where θ and λ represent the Bragg angle and incident X-ray wavelength (1.03 Å), respectively. It was observed from these XRD results that plain and Ce-doped TiO_2 samples showed no obvious diffraction peaks due either to cerium or TiO_2, except those originating from ITO substrates. Furthermore, the GAXD results indicate that all samples annealed at 200°C remained amorphous irrespective of doping concentrations.

3.3 X-ray photoelectron spectroscopy analysis

To demonstrate variations in the samples' chemical states, XPS was carried out. XPS spectra of the plain TiO_2 samples revealed the existence of elements such as Ti, O, and C; no other impurities were found. Figure 5A, further represents the XPS results of Ti 2p spectra for TiO_2 and 30% Ce-doped TiO_2 samples. In the plain TiO_2 samples, the peaks at binding energies of 458.4 and 464.1 eV are attributed to Ti $2p_{3/2}$ and Ti $2p_{1/2}$, respectively. The splitting of Ti 2p doublet around 5.7 eV indicates the presence of Ti^{4+} in the TiO_2 samples, which is consistent with other studies (Zhang et al., 2009; Zhu et al., 2017). After doping 30% of Ce into the TiO_2 samples, a shift of about 0.1 eV towards higher binding energy was observed. In addition, Ce 3days XPS spectra as shown in Figure 5B, further confirm the presence of Ce in the 30% doped samples. The existence of multiple peaks around 880–905 eV may be due to the coexistence of Ce^{3+} and Ce^{4+} oxidation states in the Ce-doped TiO_2 coating, suggesting that the sample surfaces are not fully oxidized and some oxygen vacancies in the samples might exist (Zhang et al., 2009; Zhang et al., 2012).

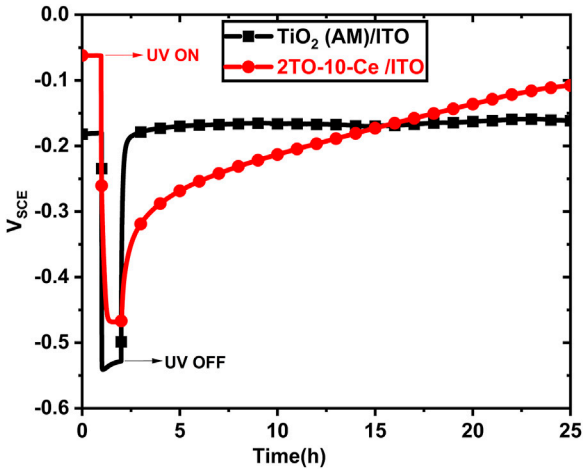

FIGURE 7
OCP responses of TiO_2 (AM)/ITO and ITO/2TO-10-Ce in the designated electrolyte solution to the absence and presence of UV illumination.

The shift of binding energy towards higher values for 30% Ce-doped TiO_2 samples in comparison with plain TiO_2 might account for the surface enrichment of the ceria leading to intermixing or the charge transfer between Ti and Ce atoms (Luo et al., 2015).

3.4 Surface analysis

The morphology and surface nature of the various layers of Ce-doped TiO_2 coatings with different Ce contents on the 304LSS substrate were analyzed by SEM, and the results are shown in Figure 6. As expected, every sample with the Ce-doped TiO_2 coating shows an excellent sealable and crack-free intact film covering the sample surface, which is consistent with previous results (Li et al., 2012). It is believed that the addition of cerium ions to the TiO_2 coating restrains crystal growth and contributes to a balance between compactness and chemical stability. Among the Ce-doped TiO_2 coatings, the one with 30% cerium showed a more homogeneous and denser distribution of cerium ions over the surface, and the corresponding EDX result reveals that the prepared coating consisted of Ti, O, and Ce elements with an atomic percent of 11.5%, 2.5%, and 2.5%, respectively. To further improve the stability and corrosion resistance of the 30% Ce-doped TiO_2 coating in the solution containing chloride ions, additional layers of plain amorphous TiO_2 were fabricated over it. Figure 6D shows the surface morphology of the 304LSS/3TO-30-Ce sample substrate. The TiO_2 coverage on the aforementioned sample was continuous and densely distributed on the outer surface of the Ce-doped TiO_2 coating. The cross section morphology and coating thickness of the 304LSS/3TO-30-Ce was determined using focused ion beam (FIB) analysis. The results showed that the thickness of the Ce doped TiO_2 coating was 442 nm and that of the amorphous TiO_2 coating was around 355 nm.

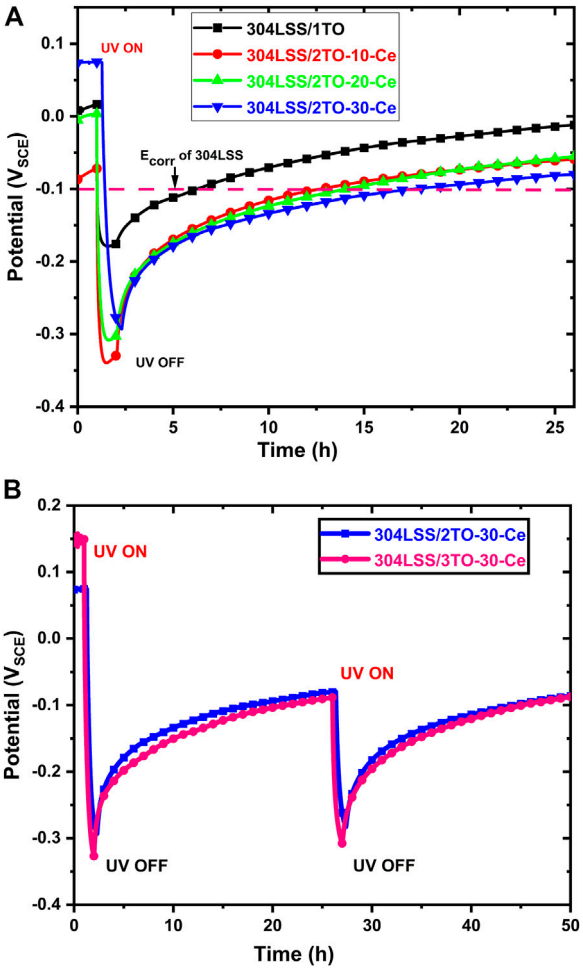

FIGURE 8
(A) OCP responses of 304LSS/1TO, 304LSS/2TO-10-Ce, 304LSS/2TO-20-Ce, 304LSS/2TO-30-Ce in the designated electrolyte solutions to the absence and presence of UV illumination and **(B)** OCP responses of 304LSS/2TO-30-Ce, 304LSS/3TO-30-Ce in the designated electrolyte solutions to the absence and presence of UV illumination for two cycles.

3.5 Photo-electrochemical responses of TiO_2-coated samples to stimulated UV illumination

The photo-cathodic protection properties of the Ce-doped TiO_2 and plain amorphous TiO_2 coatings were investigated by OCP measurements in the designated electrolyte solution of 3.5% NaCl for ITO and the 304LSS substrates.

3.5.1 Variations in OCP responses of ITO substrates coated with Ce-doped TiO_2 and plain TiO_2 coating

Before experimenting on the 304LSS substrates, we evaluated the influence of the cerium ions on the charge storage of the photogenerated electrons from the plain amorphous TiO_2 coatings to the cerium-doped TiO_2 coatings. Figure 7 compares the OCP responses of the ITO/1TO and ITO/2TO-10-Ce samples as a function of time under dark and UV-illuminated conditions.

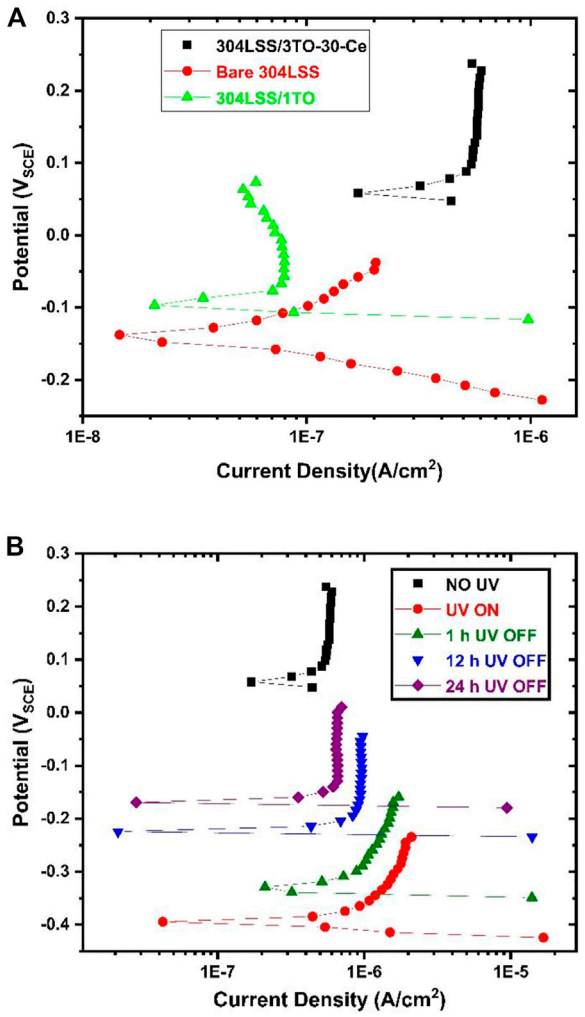

FIGURE 9
Polarization curves of the uncoated 304LSS sample, 304LSS/1TO and the 304LSS/3TO-30-Ce sample **(A)**, and polarization curves of the 304LSS/3TO-30-Ce sample prior to UV illumination, with UV illumination, and 1 h, 12 h and 24 h after cutoff of UV **(B)**.

TABLE 3 Electrochemical polarization parameters and conditions.

Condition	Synonyms
Electrochemical potential under stable equilibrium condition before UV irradiation	Dark 1
Electrochemical potential during UV irradiation for 1 h	Light
Electrochemical potential after 1 h of UV irradiation off	Dark 2
Electrochemical potential after 12 h of UV irradiation off	Dark 3
Electrochemical potential after 24 h of UV irradiation off	Dark 4

Before starting UV illumination, the OCP of the two samples were stabilized near −0.1 V_{SCE}. After beginning UV illumination, we observed that the OCPs of both samples showed a remarkable negative shift to more active values of electrochemical potential, exhibiting an n-type photocatalytic effect due to the generation of photoelectrons from the TiO_2 coatings. It was found that while the sample ITO (AM)/1TO tends to sustain a more stable OCP value at −0.52 V_{SCE}, once the UV illumination is turned off, the OCP values returned quickly to their original value before UV illumination since the free electrons started to recombine with their charge carriers. This result indicates that the plain TiO_2 coating exhibited excellent photocatalytic activity in generating free electrons. However, the TiO_2 coatings stopped offering corrosion protection during dark conditions due to their inability to trap and store the generated free electrons under UV illumination (Sathasivam et al., 2022). Nevertheless, the sample ITO/2TO-10-Ce gave results that contrasted with those of the ITO/1TO. It is anticipated that the introduction of a Ce-doped TiO_2 coating underneath the plain amorphous TiO_2 coating may serve as an electron storage pool for the excess photogenerated electrons from the TiO_2 coating. As shown in Figure 7, the OCP of ITO/2TO-10-Ce stabilized around −0.47 V_{SCE}, which is slightly less than that of the sample ITO/1TO under UV illumination. It should be noted that incorporating cerium into the TiO_2 coating, even in trace amounts, negatively impacted the photocatalytic activity of the TiO_2 coating. Furthermore, after illuminating the coating for 1 h, it was observed that the OCP of the ITO/2TO-10-Ce sample exhibited a slow recovery in the electrode potential on stopping the UV illumination. This indicates that the Ce-doped TiO_2 coating contained the redox couple Ce^{4+}/Ce^{3+}, in which Ce^{4+} ions serve as a trap for the photogenerated electrons and are reduced to Ce^{3+} ions under UV illumination. The electrons captured by Ce^{3+} are released slowly, to return to Ce^{4+} ions in the absence of UV illumination (Yang and Cheng, 2017). Moreover, the space charge layer of the amorphous TiO_2 coating is thicker, rendering it more difficult for the stored electrons to escape from the Ce-doped TiO_2 coating in the absence of UV illumination. The results show that this specifically developed multilayered Ce-doped TiO_2 coating pattern possesses a unique charge storage property that helps to retain the photo cathodic protection effect even without UV illumination and maintains a noble electrode potential for more than 24 h under aerated conditions.

While the concentration of the Ce dopant in the TiO_2 played a crucial role in the efficient charge storage property, increasing its concentration over a certain amount favored the recombination of the charge carrier, resulting in a decline in the photocatalytic effect of the TiO_2 coatings. Therefore, a critical concentration limit of the Ce dopant must be maintained to achieve maximum efficiency of the photocathodic protection of the 304LSS in the absence of UV illumination (Subasri et al., 2010).

3.5.2 Variations in OCP responses of 304LSS substrates coated with Ce-doped TiO_2 and plain TiO_2 coating

The time evolution of the OCP variation of the samples with different concentrations of the cerium-doped TiO_2 coating on 304LSS and designated as 304LSS/2TO-10-Ce, 304LSS/2TO-20-Ce, 304LSS/2TO-30-Ce under the presence and absence of UV illumination are illustrated in Figure 8A. Before initiating UV illumination, all of the samples showed a stable OCP around 0 V_{SCE}, which is slightly higher than the OCP of the bare 304LSS (shown as a dotted line in Figure 8A). It was observed that, as a result

of the sudden generation of charge carriers from the overlaid amorphous TiO_2 coating, the OCPs of all samples had an abrupt cathodic shift after UV illumination to the more active values than the bare 304LSS. For 304LSS/1TO, the decrease in OCP upon UV illumination is distinctly less than those of the other samples. Among the Ce doped TiO_2 samples, the OCP of 304LSS/2TO-30-Ce showed a minimum active potential of −0.29 V_{SCE} than the other two. This is due to the higher concentrations of cerium in the TiO_2 coating generating more photogenerated electrons, which were stored in the Ce-doped layer and resulted in the decline of the potential reduction. However, the OCP of 304LSS/2TO-30-Ce rose at a slow rate to the initial potential once the UV illumination was turned off. The overlaid amorphous TiO_2 coating caused this slow recovery, taking almost 12 h to reach the OCP value of the bare 304LSS and due in part to the suppression of the oxygen reduction reaction (Huang et al., 1998). Further, the addition of one more layer of amorphous TiO_2 coating in the sample 304LSS/2TO-30-Ce seemed to enhance the photocatalytic effect and resulted in a higher negative potential, which in turn promoted the OCP recovery time to more than 24 h once the UV illumination was turned off. The time evolution of the OCP variation experiments was investigated for several cycles over the 304LSS/2TO-30-Ce 304LSS/3TO-30-Ce specimens and the results showed good durability in the photoelectrochemical characteristics of the coatings (see Figure 8B).

3.6 Corrosion rates of TiO_2-coated samples

Electrochemical polarization analysis was conducted to investigate the corrosion resistance of a various layers of TiO_2 coated and uncoated 304LSS sample exposed to an aerated 3.5% sodium chloride electrolyte solution in the absence of UV illumination (see Figure 9A). Before each round of polarization analysis, an electrolyte solution was thoroughly purged with air for 20 min. The sample was then immersed in the solution for 3 h until a stabilized equilibrium was reached. The results showed that the electrochemical corrosion potential (ECP) of the TiO_2 coated samples were much higher than that of the uncoated 304LSS sample. The corrosion current density of the uncoated sample was 3.02×10^{-8} A/cm^2. In the meantime the 304LSS/1TO sample with only one layer of amorphous TiO_2 coating exhibited a lower anodic current density than the bare one, even in the absence of UV illumination. However, the 304LSS/3TO-30-Ce sample had a significantly higher anodic current density of 1.70×10^{-5} A/cm^2. During the polarization analysis the potential scanning direction of the current from the active potential to the noble side led to initiation of Ce^{3+} oxidation to Ce^{4+}, which resulted in the higher anodic current density for the 304LSS/3TO-30-Ce sample, consistent with what was observed in a previous study (Sonar et al., 2022).

Figure 9B shows the samples' comparative polarization curves under different conditions in the absence and presence of UV illumination. Table 3 summarizes the test conditions. In the presence of UV illumination, photocatalytic reactions occurred at the surface of the sample, showing a noticeable cathodic shift in electrochemical corrosion potential. This was more active than in the uncoated sample, signifying an accumulation of photogenerated electrons. Accordingly, the corresponding corrosion current density was significantly lowered to 7.15×10^{-12} A/cm^2. It should be noted that the increase in the anodic current density can be ascribed to the release of the photogenerated electrons from the space charge layer. For the same sample discussed in the preceding section, the ECP change was in good agreement with the OCP variation. To estimate the time-dependent variation in the electrochemical corrosion potential concerning the samples' corresponding corrosion current density, polarization analyses were conducted at 1 h, 12 h, and 24 h after UV illumination was turned off. The sample's ECP shows a notable increase in potential after 1 h, which further increased after 10 h and 24 h. This was consistent with the sample's OCP variations discussed in the previous section. The samples' respective corrosion densities were estimated to be around 6.10×10^{-11} A/cm^2 after 1 h, and 2.47×10^{-9} A/cm^2, 1.06×10^{-8} A/cm^2 after 12 h and 24 h respectively. This outcome indicates that the coated sample's corrosion current density could last one order of magnitude less than that of the uncoated sample, even after 24 h in the absence of UV. This suggests the retention of cathodic protection of the metal alloy by using a specifically designed multilayered TiO_2 coating.

4 Conclusion

A multilayered Ce-doped TiO_2 coating with charge capability was fabricated over 304LSS using a sol-gel process combined with annealing at low temperatures. Coupled with UV illumination, this technique could be used as a corrosion mitigation measure for structural materials used in dry storage canisters near offshore platforms in the presence of chloride ions. These specialized TiO_2 coatings produced a greater photocatalytic effect on 304LSS, resulting in a lowering of the electrochemical potential as well as the corrosion current density in a corrosive medium of 3.5% NaCl solution. This indicates that Ce-doped TiO_2 coatings have a charge storage capability that offers extended photo-cathodic protection for the metal alloy for more than 24 h even after UV illumination was turned off.

Data availability statement

The raw data supporting the conclusions of this article will be made available by the authors, without undue reservation.

Author contributions

KS, investigation, formal analysis, methodology, writing—original draft. MW, supervision, resources, funding acquisition, and project administration. AA, investigation and formal analysis. C-HL, supervision, resources. T-KY, supervision, conceptualization, data curation, writing - review and editing.

Acknowledgments

The authors wish to thank Taiwan International Graduate Program of Academia Sinica for a part of funding support. The beam time provided by National Synchrotron Radiation Research Center is also highly acknowledged. We are grateful to thank Ms.

See-Lan Cheah (The Instrumentation Center at NTHU) for the HRXPS analysis.

Conflict of interest

The authors declare that the research was conducted in the absence of any commercial or financial relationships that could be construed as a potential conflict of interest.

Publisher's note

All claims expressed in this article are solely those of the authors and do not necessarily represent those of their affiliated organizations, or those of the publisher, the editors and the reviewers. Any product that may be evaluated in this article, or claim that may be made by its manufacturer, is not guaranteed or endorsed by the publisher.

References

Huang, J., Konishi, T., Shinohara, T., and Tsujikawa, S. (1998). Sol-gel derived Ti-Fe oxide coating for photoelectrochemical cathodic protection of carbon steel. *Zairyo-to-Kankyo* 47, 193–199. doi:10.3323/jcorr1991.47.193

Li, J., Lin, C.-J., Lai, Y.-K., and Du, R.-G. (2010). Photogenerated cathodic protection of flower-like, nanostructured, N-doped TiO2 film on stainless steel. *Surf. Coatings Technol.* 205, 557–564. doi:10.1016/j.surfcoat.2010.07.030

Li, M., Luo, S., Wu, P., and Shen, J. (2005). Photocathodic protection effect of TiO_2 films for carbon steel in 3% NaCl solutions. *Electrochimica Acta* 50, 3401–3406. doi:10.1016/j.electacta.2004.12.031

Li, S., Wang, Q., Chen, T., Zhou, Z., Wang, Y., and Fu, J. (2012). Study on cerium-doped nano-TiO2 coatings for corrosion protection of 316 L stainless steel. *Nanoscale Res. Lett.* 7, 227–229. doi:10.1186/1556-276X-7-227

Liu, Y., Xu, C., and Feng, Z. (2014). Characteristics and anticorrosion performance of Fe-doped TiO_2 films by liquid phase deposition method. *Appl. Surf. Sci.* 314, 392–399. doi:10.1016/j.apsusc.2014.07.042

Luo, S., Nguyen-Phan, T.-D., Johnston-Peck, A. C., Barrio, L., Sallis, S., Arena, D. A., et al. (2015). Hierarchical heterogeneity at the CeOx–TiO2 interface: Electronic and geometric structural influence on the photocatalytic activity of oxide on oxide nanostructures. *J. Phys. Chem. C* 119, 2669–2679. doi:10.1021/jp511986n

Momeni, M. M., and Motalebian, M. (2021). Chromium-doped titanium oxide nanotubes grown via one-step anodization for efficient photocathodic protection of stainless steel. *Surf. Coatings Technol.* 420, 127304. doi:10.1016/j.surfcoat.2021.127304

Padmanathan, N., and Selladurai, S. (2014). Shape controlled synthesis of CeO_2 nanostructures for high performance supercapacitor electrodes. *RSC Adv.* 4, 6527–6534. doi:10.1039/C3RA43339K

Peng, Y., Hughes, A. E., Deacon, G. B., Junk, P. C., Hinton, B. R. W., Forsyth, M., et al. (2018). A study of rare-earth 3-(4-methylbenzoyl)-propanoate compounds as corrosion inhibitors for AS1020 mild steel in NaCl solutions. *Corros. Sci.* 145, 199–211. doi:10.1016/j.corsci.2018.09.022

Saito, S. (2010). Role of nuclear energy to a future society of shortage of energy resources and global warming. *J. Nucl. Mater.* 398, 1–9. doi:10.1016/j.jnucmat.2009.10.002

Sathasivam, K., Wang, M.-Y., Anbalagan, A. K., Lee, C.-H., and Yeh, T.-K. (2022). Prolonged and enhanced protection against corrosion over titanium oxide-coated 304L stainless steels having been irradiated with ultraviolet. *Front. Mater.* 9. doi:10.3389/fmats.2022.863603

Shinohara, T. (2001). Impedance measurement for slow decline of electrode potential of Fe-doped TiO_2 coating. *Zairyo-to-Kankyo* 50, 170–176. doi:10.3323/jcorr1991.50.170

Sonar, P. A., Sanjeevagol, S. G., Manjanna, J., Patake, V. D., and Nitin, S. (2022). Electrochemical behavior of cerium (III) hydroxide thin-film electrode in aqueous and non-aqueous electrolyte for supercapacitor applications. *J. Mater. Sci. Mater. Electron.* 33, 25787–25795. doi:10.1007/s10854-022-09270-x

Subasri, R., and Shinohara, T. (2004). Application of the photoeffect in TiO_2 for cathodic protection of copper. *Electrochemistry* 72, 880–884. doi:10.5796/electrochemistry.72.880

Subasri, R., and Shinohara, T. (2003). Investigations on SnO_2–TiO_2 composite photoelectrodes for corrosion protection. *Electrochem. Commun.* 5, 897–902. doi:10.1016/j.elecom.2003.08.016

Subasri, R., Tripathi, M., Murugan, K., Revathi, J., Rao, G. V. N., and Rao, T. N. (2010). Investigations on the photocatalytic activity of sol–gel derived plain and Fe^{3+}/Nb^{5+}-doped titania coatings on glass substrates. *Mater. Chem. Phys.* 124, 63–68. doi:10.1016/j.matchemphys.2010.08.013

Tong, T., Zhang, J., Tian, B., Chen, F., He, D., and Anpo, M. (2007). Preparation of Ce–TiO_2 catalysts by controlled hydrolysis of titanium alkoxide based on esterification reaction and study on its photocatalytic activity. *J. Colloid Interface Sci.* 315, 382–388. doi:10.1016/j.jcis.2007.06.051

Wang, W.-Y., Tseng, Y.-S., and Yeh, T.-K. (2020). Evaluation of crack growth of chloride-induced stress corrosion cracking in dry storage system under different environmental conditions. *Prog. Nucl. Energy* 130, 103534. doi:10.1016/j.pnucene.2020.103534

Wang, W.-Y., Tseng, Y.-S., and Yeh, T.-K. (2022). Tolerance assessment and crack growth of chloride-induced stress corrosion cracking for Chinshan dry storage system. *Prog. Nucl. Energy* 147, 104210. doi:10.1016/j.pnucene.2022.104210

Yang, Y., and Cheng, Y. F. (2017). Bi-layered CeO_2/$SrTiO_3$ nanocomposite photoelectrode for energy storage and photocathodic protection. *Electrochimica Acta* 253, 134–141. doi:10.1016/j.electacta.2017.09.044

Yeom, H., Dabney, T., Pocquette, N., Ross, K., Pfefferkorn, F. E., and Sridharan, K. (2020). Cold spray deposition of 304L stainless steel to mitigate chloride-induced stress corrosion cracking in canisters for used nuclear fuel storage. *J. Nucl. Mater.* 538, 152254. doi:10.1016/j.jnucmat.2020.152254

Yeom, H., and Sridharan, K. (2021). Cold spray technology in nuclear energy applications: A review of recent advances. *Ann. Nucl. Energy* 150, 107835. doi:10.1016/j.anucene.2020.107835

Zhang, J., Peng, W., Chen, Z., Chen, H., and Han, L. (2012). Effect of cerium doping in the TiO_2 photoanode on the electron transport of dye-sensitized solar cells. *J. Phys. Chem. C* 116, 19182–19190. doi:10.1021/jp3060735

Zhang, Q., Huang, Y., Blackwood, D. J., Zhang, B., Lu, D., Yang, D., et al. (2020). On the long term estimation of hydrogen embrittlement risks of titanium for the fabrication of nuclear waste container in bentonite buffer of nuclear waste repository. *J. Nucl. Mater.* 533, 152092. doi:10.1016/j.jnucmat.2020.152092

Zhang, Y., Yuwono, A. H., Wang, J., and Li, J. (2009). Enhanced photocatalysis by doping cerium into mesoporous titania thin films. *J. Phys. Chem. C* 113, 21406–21412. doi:10.1021/jp907901k

Zhu, L., Lu, Q., Lv, L., Wang, Y., Hu, Y., Deng, Z., et al. (2017). Ligand-free rutile and anatase TiO_2 nanocrystals as electron extraction layers for high performance inverted polymer solar cells. *RSC Adv.* 7, 20084–20092. doi:10.1039/C7RA00134G